

**Excitonic states in CdTe/Cd<sub>0.74</sub>Mg<sub>0.26</sub>Te quantum wires grown on vicinal substrates**

Seiji Nagahara,\* Takashi Kita, and Osamu Wada

*Department of Electrical and Electronics Engineering, Faculty of Engineering, Kobe University, Rokkodai 1-1, Nada, Kobe 657-8501, Japan*

Laurent Marsal and Henri Mariette

*Laboratoire de Spectrometrie Physique, Universite J. Fourier, Grenoble I, CNRS (UMR 5588), Boîte Postal 87, F-38402 Saint Martin d'Herès Cedex, France*

(Received 6 March 2002; revised manuscript received 28 August 2002; published 4 February 2003)

We have investigated excitonic luminescence from CdTe/Cd<sub>0.74</sub>Mg<sub>0.26</sub>Te quantum wires (QWR's) grown on vicinal substrates. The temperature dependence of the radiative lifetime of one-dimensional exciton in the QWR's was measured using time-resolved spectroscopy. The results are compared with that of two-dimensional exciton in CdTe/Cd<sub>0.74</sub>Mg<sub>0.26</sub>Te quantum well (QW). The radiative lifetimes of one-dimensional exciton in the QWR's and two-dimensional exciton in the QW increase with  $T$  but show clearly different behavior. The observed radiative lifetime in the QWR's obeys  $T^{1/2}$  in a wide temperature range, confirming the one-dimensional nature in exciton thermalization. On the other hand, the radiative lifetime in the QW is linear with  $T$ . Furthermore, we observed clear biexciton formation at  $\leq 10$  K in the QWR's. The biexciton binding energy estimated from the line-shape analysis of the luminescence spectra for the QWR's is 5.2 meV.

DOI: 10.1103/PhysRevB.67.085301

PACS number(s): 78.55.Et; 78.66.Hf

**I. INTRODUCTION**

One-dimensional (1D) quantum wire (QWR) structures have attracted great attention for optoelectronic device applications, since superior optical and electrical properties are predicted theoretically.<sup>1-3</sup> The reduced dimension leads to pronounce excitonic effects due to an enhanced spatial overlap of the electron and hole wave functions. Different approaches such as lithography,<sup>4</sup> growth on prepatterned substrates,<sup>5-8</sup> and cleaved-edge overgrowth<sup>9-11</sup> have been performed to fabricate QWR structures. In contrast to these man-made structures, self-organized growths of low-dimensional structures such as QWR (Refs. 12-18) and quantum dot<sup>19</sup> have been demonstrated, because of their simple technological step for the growth process. Organized growth of semiconductors on vicinal substrate is expected to realize an array of QWR's; the repeated deposition of a fractional monolayer (ML)  $m$  of material  $A$  followed by a fractional ML  $n$  of material  $B$  results in the array of QWR's, also called a  $A_m B_n$  tilted superlattice. The lateral scale can be controlled by the substrate off angle, and a lateral confinement potential depends on the degree of modulation of the lateral composition. At  $m$  and  $n = 0.5$ , the cross section of the QWR's becomes square. When  $m$  is not equal to  $n$ , the shape of the cross section tilts from the growth direction.

The temporal evolution of the luminescence, e.g., free exciton ( $X$ ) or biexciton ( $XX$ ) luminescence, can be useful as a monitor of the population of respective species in low-dimensional systems. It is generally known that linear increase of the interband recombination time with the temperature is sometimes used to argue that the recombination of  $X$  in quantum wells (QW's) is essentially radiative.<sup>20-24</sup> Evaluation of the intrinsic radiative lifetime in nanostructures relies on such measurement, although in real heterostructures, it is difficult to observe the intrinsic radiative lifetime directly due to localization of the  $X$ . In contrast with the two-

dimensional (2D)  $X$  in QW's, properties of the 1D  $X$  in QWR's were presented theoretically by Citrin.<sup>25</sup> A very important result for the 1D  $X$  is a long intrinsic radiative lifetime due to the finite spatial coherence in the lateral direction and a  $T^{1/2}$  dependence of the effective lifetime due to thermalization effects. In the previous experiments on V-groove GaAs QWR's (Ref. 8) and on cleaved-edge overgrown GaAs QWR's,<sup>9</sup> the intrinsic radiative lifetimes have been estimated from such temperature dependence. In contrast to the III-V materials, the II-VI materials exhibit significantly larger  $X$  binding energies, e.g., 24 meV for 6.5-nm-wide CdTe/Cd<sub>0.51</sub>Mg<sub>0.49</sub>Te QW.<sup>26</sup> In our recent paper,<sup>27</sup> we have reported the observation of such 1D behavior in CdTe/Cd<sub>0.74</sub>Mg<sub>0.26</sub>Te QWR structures grown on vicinal substrates, in which the samples are excited above the Cd<sub>0.74</sub>Mg<sub>0.26</sub>Te barrier. In this study, detailed measurements of temporal evolution of photoluminescence (PL) under below-barrier excitation are performed to avoid energy relaxation from the barrier into the wire. The observed radiative lifetimes in the QWR's is typical of  $X$  thermalization in the 1D systems, which obeys  $T^{1/2}$  at  $\geq 10$  K. At low temperature  $\leq 10$  K, however, the radiative lifetime seems to deviate from the  $T^{1/2}$  dependence, for which we found  $XX$  PL on the low-energy side of the  $X$  PL.

**II. EXPERIMENTS**

The growth of lateral superlattice on the vicinal surface is based on the step-flow growth of fractional ML's over a very regular array of monomolecular steps. The steps align along the [010] direction. In this experiment, the array of CdTe/Cd<sub>0.74</sub>Mg<sub>0.26</sub>Te QWR's, with  $m$  and  $n \approx 0.5$ , was grown on Cd<sub>0.96</sub>Zn<sub>0.04</sub>Te (001) substrates misoriented 1° toward the [100] direction by molecular beam epitaxy (MBE).<sup>28</sup> A repeated deposition of a fractional ML  $m$  of CdTe followed by a fractional ML  $n$  of Cd<sub>0.74</sub>Mg<sub>0.26</sub>Te resulted in

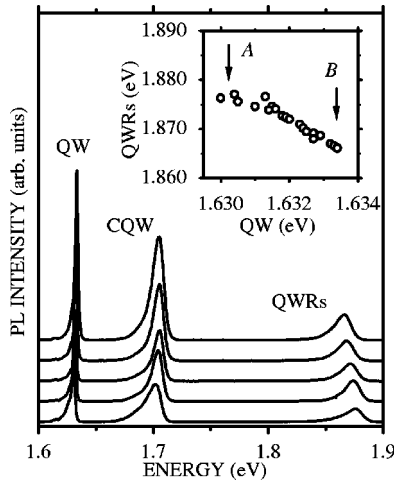


FIG. 1. PL spectra at various positions on the sample at 13.6 K. The inset shows the PL peak energy of CdTe/Cd<sub>0.74</sub>Mg<sub>0.26</sub>Te QWR's as a function of that of CdTe/Cd<sub>0.74</sub>Mg<sub>0.26</sub>Te QW. The points A and B correspond to the tilted angles of  $\approx 55^\circ$  and  $\approx 0^\circ$ , respectively.

CdTe/Cd<sub>0.74</sub>Mg<sub>0.26</sub>Te QWR's. This cycle was repeated 30 times. As a consequence, the  $1^\circ$  misoriented substrate gave rise to approximately square wires of  $9.3 \text{ nm} \times 9.7 \text{ nm}$ .<sup>27</sup> A considerable flux intensity gradient in the MBE resulted in tilted square cross section of the QWR's. The tilt angle  $\theta$  that is defined as the angle from the [001] direction varies for given positions on the sample. After growing the QWR's itself, a single CdTe quantum well (QW) with 25-ML thickness and a coupled QW (CQW) consisting of two 12-ML CdTe QW separated by one ML of MgTe were grown.

Continuous wave (CW) PL and its excitation (PLE) measurements were performed under the excitation by the 488 nm line of an Ar-ion laser and monochromatic light of a tungsten lamp, respectively. Time resolved spectroscopy of the radiative recombination of X was performed at 2.5 K in a He-gas-flow cryostat using 250-fs pulses from doubler of an optical parametric oscillator excited by a mode-locked Ti:sapphire laser. The repetition rate was 80 MHz, and the laser wavelength was 620 nm. This excitation energy is lower than the Cd<sub>0.74</sub>Mg<sub>0.26</sub>Te barrier potential, which avoids energy relaxation from the barrier. The laser spot diameter was about  $100 \mu\text{m}$ . The time-resolved PL was dispersed in a 0.25-m monochromator and detected with spectral and temporal resolution of 0.15 nm and about 2 ps, respectively, by using a streak camera with two-dimensional readout.

### III. RESULTS AND DISCUSSION

#### A. 1D X recombination

Figure 1 shows CW-PL spectra taken at various positions on the sample at 13.6 K. The laser spot diameter was about  $50 \mu\text{m}$ . Three peaks being attributed to X recombinations between the ground electron ( $E_1$ ) and heavy-hole ( $\text{HH}_1$ ) states in the QW, CQW, and QWR's are clearly observed. The inset shows the relation between the PL peak energies for the QWR's and QW. The large flux of CdTe and

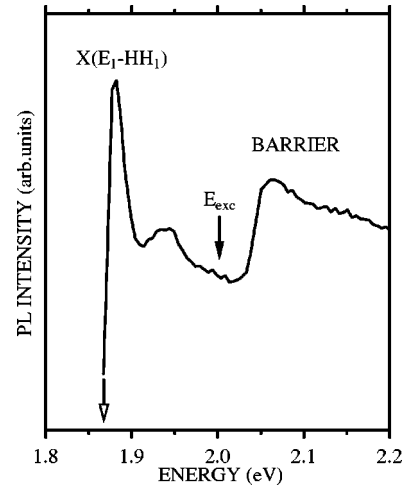


FIG. 2. PLE spectra taken at the point B at 3.8 K.

Cd<sub>0.74</sub>Mg<sub>0.26</sub>Te gives rise to an increase of the tilt angle  $\theta$ . With increasing  $\theta$ , the PL peak of the QWR's shifts toward the higher energy side due to narrowing of the lateral confinement, while the PL peaks of the QW and CQW shift toward the lower energy side. Since the lattice mismatch between CdTe and Cd<sub>0.74</sub>Mg<sub>0.26</sub>Te is about 0.3%, the energy shift of PL peak due to strain is negligible. The X-transition energy of the  $E_1\text{-HH}_1$  as a function of  $\theta$  was calculated by a theoretical approach,<sup>27</sup> from which  $\theta$  at the points A and B shown in the inset of Fig. 1 correspond to  $\approx 55^\circ$  and  $\approx 0^\circ$ , respectively. (See also Fig. 4 for illustration of QWR cross sections.)

Figure 2 shows a PLE spectrum of the QWR's at the point B. The sample temperature was 3.8 K. The PL intensity was

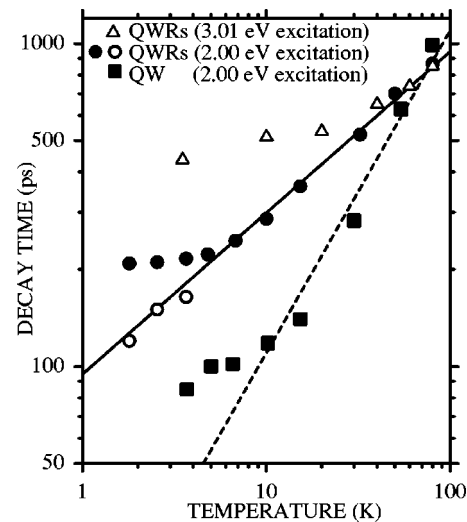


FIG. 3. Radiative lifetime of X as a function of temperature, where solid circles and squares indicate the measurement results for CdTe/Cd<sub>0.74</sub>Mg<sub>0.26</sub>Te QWR's and QW under below-barrier (2.00 eV) excitation, respectively. Open triangles plot data for the QWR's under above-barrier (3.01 eV) excitation (Ref. 27). The measurements were performed at the point B. Radiative lifetimes evaluated from the line-shape analysis are plotted by open circles. Solid and dashed lines show the  $T^{1/2}$  and  $T$  dependences, respectively.

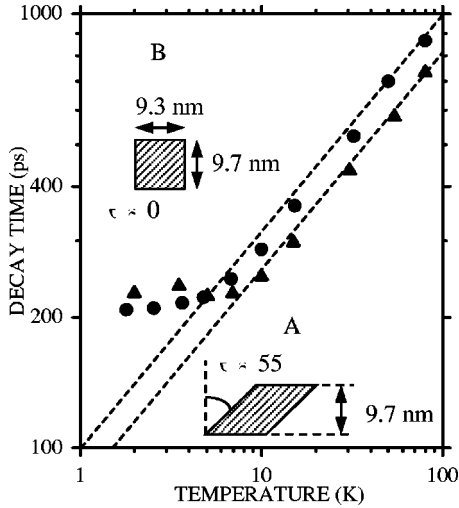


FIG. 4. Radiative lifetimes of  $X$  measured at the point A (solid triangles) and B (solid circles) as a function of temperature. Dashed lines show the  $T^{1/2}$  dependence. The insets show the sketch of CdTe/Cd<sub>0.74</sub>Mg<sub>0.26</sub>Te QWR's at the point A and B.

detected at 1.867 eV indicated by an open arrow. A strong excitonic absorptions is observed at 1.877 eV. This corresponds to the  $X$  transition between the  $E_1$  and  $HH_1$  states. Relatively broad resonances considered to be due to transitions related to the excited electron states and the hole states are observed near 1.94 eV.<sup>29–31</sup> The absorption edge due to the continuum state of the Cd<sub>0.74</sub>Mg<sub>0.26</sub>Te barrier appears above 2.05 eV. The excitation energy used in the following time-resolved measurements is indicated by a solid arrow.

The temperature dependence of the radiative lifetime of the 1D  $X$  in the QWR's and 2D  $X$  in the QW are plotted by solid circles and squares in Fig. 3, respectively. The radiative lifetime was evaluated from the decay profile at the peak position of the time-integrated PL spectrum. The measurement was performed at the point B. The excitation intensity is 0.96  $\mu\text{J}/\text{cm}^2$ . We also plot data for the QWR's (open triangles) obtained under the above-barrier (3.01 eV) excitation.<sup>27</sup> The radiative lifetimes for the 1D- and 2D- $X$  recombination increase with temperature  $T$  but show clearly different behavior. The radiative lifetime under the below-barrier (2.00 eV) excitation for the QW increases linearly with temperature at  $\geq 10$  K. This trend has been reported in many papers.<sup>20–23</sup> When the temperature increases, the fraction of  $X$  that can participate in the recombination process decreases, and its radiative lifetime becomes long. In the 2D-QW system, the fraction of  $X$  with small kinetic energy is inversely proportional to  $T$ , because of the Maxwell-Boltzmann distribution of  $X$  in the 2D density of states.<sup>32</sup> Therefore, the radiative lifetime of  $X$  in the QW shows a linear increase with the temperature. A dashed line in Fig. 3 indicates the  $T$  dependence. On the other hand, the temperature dependence of the radiative lifetime in the QWR's is small. The small temperature dependence can be ascribed to the 1D density of state and thermalization in it. Citrin suggested that the radiative lifetime in the 1D density of states would obey  $T^{1/2}$ .<sup>25</sup> The solid line in Fig. 3 indicates the  $T^{1/2}$  dependence. The observed temperature dependence of the

radiative lifetime under the below-barrier (2.00 eV) excitation of the QWR's is proportional to  $T^{1/2}$  at  $\geq 10$  K, though the radiative lifetime under the above-barrier (3.01 eV) excitation shows agreement with the  $T^{1/2}$  dependence only at  $\geq 40$  K. The relatively large deviation of the radiative lifetimes under the above-barrier (3.01 eV) excitation from the  $T^{1/2}$  dependence is considered to be due to the energy relaxation process of photoexcited carriers from the barrier into the wire. In this paper, we consider the data obtained under the below-barrier (2.00 eV) excitation in order to avoid the energy relaxation from the barrier. At temperature lower than 10 K, a new PL (NPL) (to be discussed later in Sec. III B) appears in addition to the  $X$  PL. This leads to a deviation of the low-temperature total signal from the high-temperature trend. However, a deconvolution of the total signal into the excitonic and NPL contributions shows that the excitonic contribution (open circles) follows the expected behavior also at  $\leq 10$  K. This point is discussed in detail in the next subsection.

The effective radiative lifetime is given by<sup>7</sup>

$$\tau_{1D}(T) \approx \tau_0 \sqrt{\frac{\pi k_B T}{4\Delta}} \quad (1)$$

for 1D and

$$\tau_{2D}(T) \approx \tau_0 \frac{k_B T}{\Delta} \quad (2)$$

for 2D, where  $\tau_0$  is the intrinsic radiative lifetime of the  $X$  at  $k \approx 0$ , and  $\Delta = \hbar^2 k_0^2 / 2M$  the kinetic energy of  $X$  that can recombine. Here  $k_0$  is the in-plane wave vector given by  $2\pi n / \lambda$ , where  $n$  is refractive index and  $\lambda$  the PL wavelength.  $M$  is the in-plane mass of the  $X$ . The observed radiative lifetimes in the QWR's and the QW are expressed as 100  $T^{1/2}$  ps  $\text{K}^{-1/2}$  and 11  $T$  ps  $\text{K}^{-1}$ . Then, according to Eqs. (1) and (2), the values of  $\tau_0$  for the QWR's and QW are found to be 72 and 5 ps, respectively. The long  $\tau_0$  in the QWR's is due to the decrease of the  $X$  coherence length imposed by the lateral confinement in the QWR structure.

Furthermore, we compared the radiative lifetimes at the points A ( $\theta \approx 55^\circ$ ) and B ( $\theta \approx 0^\circ$ ) in Fig. 4. Solid triangles plot the radiative lifetime at the point A. The temperature dependence of the radiative lifetimes at the point A is expressed as 80  $T^{1/2}$  ps  $\text{K}^{-1/2}$ . Then, the estimated  $\tau_0$  is 59 ps, which is smaller than the value at the point B. The reduction of the  $\tau_0$  means that the larger  $\theta$  causes a longer  $X$ -coherence length. The cross section of the QWR at the point A is rhombic with  $\theta \approx 55^\circ$  as shown in the inset of Fig. 4. The observed result suggests that the rhombic size is still small enough to exhibit the 1D excitonic properties.

### B. New luminescence at $\lesssim 10$ K

As shown in Fig. 3, at low temperature  $\lesssim 10$  K, the radiative lifetimes in the QWR's and QW deviate from the  $T^{1/2}$  and  $T$  dependences, respectively. Figure 5 shows the PL spectra of the QWR's measured in this temperature range. The excitation intensity is 0.96  $\mu\text{J}/\text{cm}^2$ . Below  $\approx 15$  K, the PL peak seems to shift toward the lower energy side because

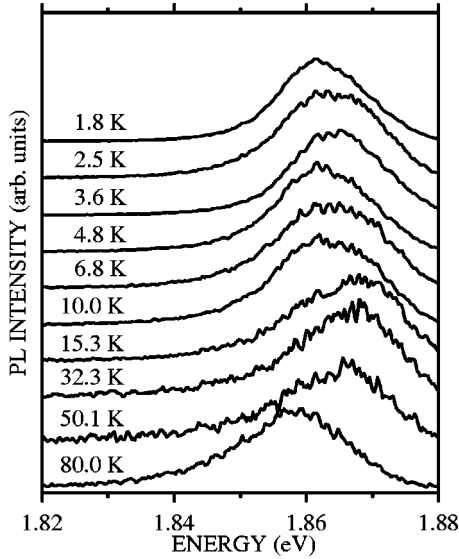


FIG. 5. PL spectra of CdTe/Cd<sub>0.74</sub>Mg<sub>0.26</sub>Te QWR's measured in a range from 1.8 to 80 K.

a new signal NPL appears at the lower energy side of the X PL. To investigate the origin of the NPL, we measured excitation power dependence of the NPL at 2.5 K. Figure 6 shows the PL spectra of the QWR's measured at various excitation intensities, where  $I_0 = 0.72 \mu\text{J}/\text{cm}^2$ . The open circle is the measured data. The NPL at 1.856 eV is enhanced at high excitation intensities. This result excludes the possibility of localized states for the NPL. A similar NPL was also observed in the QW. Several origins such as  $XX$  and trions ( $X^*$ ), i.e., negatively or positively charged excitons, for the

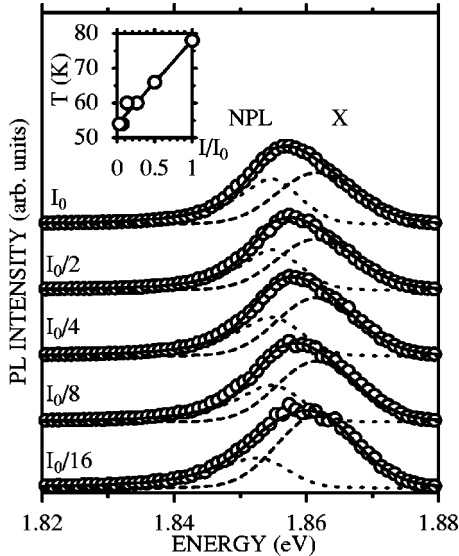


FIG. 6. PL spectra of CdTe/Cd<sub>0.74</sub>Mg<sub>0.26</sub>Te QWR's at 2.5 K measured at various excitation intensities. Open circles plot the measurement data.  $I_0 = 0.72 \mu\text{J}/\text{cm}^2$ . Dashed and dotted curves are the plot of X PL and NPL component estimated from the line-shape analysis, respectively. Solid curves plot the total line shape. The inset shows the temperature ( $T$ ) estimated at these excitation intensities.

NPL can be proposed. Especially,  $XX$  (Refs. 33–43) and  $X^*$  (Refs. 44–48) have been observed in many II-VI materials because of their relatively larger binding energy. Since our sample is undoped, photoexcited excess carriers may cause  $X^*$  PL.<sup>44,48</sup> Here, we focus on the  $XX$  and  $X^*$  formations to analyze the NPL.

We performed a deconvolution between the  $X$  (Boltzmann distribution) and the  $XX$  ( $X^*$ ) (reverse Boltzmann distribution).<sup>43</sup> The  $XX$  (Refs. 33–37,49) and  $X^*$  (Refs. 42,46) show similar line shapes reflecting the reverse Boltzmann distribution and the density of states, because all  $XX$  ( $X^*$ ) states are radiative. We fit the PL data with the line shape of the 1D density of states

$$I(E) \propto \int_0^{\infty} \exp\{-(E_X - E_b - E - x)^2/\Gamma^2\} \times \exp(-x/k_B T) x^{-1/2} dx, \quad (3)$$

where  $E$  is the photon energy,  $E_X$  the  $X$  energy,  $E_b$  the binding energy, and  $\Gamma$  a broadening parameter for the density of states.  $T$  for  $XX$  and  $X^*$  is equal to  $T_{\text{eff}}$  and  $M_X T_{\text{eff}}/m_*$ , respectively, where  $T_{\text{eff}}$  is the effective temperature,  $m_*$  the electron ( $m_e$ ) or hole ( $m_h$ ) mass,  $M_X$  the  $X$  mass  $m_e + m_h$ . On the other hand, the line shape of the  $X$  PL is given by the Boltzmann distribution in the density of states broadened with Gaussian. Dashed and dotted curves in Fig. 6 plot the  $X$  PL and NPL components, respectively. The line shapes including both components are indicated by solid lines in Fig. 6, which agree well with the experimental data plotted by the open circles.  $T$  in Eq. (3), which is proportional to the effective temperature, obtained from the line-shape fitting at different excitation intensities are plotted in the inset of Fig. 6. The result shows the expected increase with the excitation intensity, which is due to the randomization of momentum left behind in the center-of-mass motion of the  $X$ .<sup>34</sup> The binding energy  $E_b$  estimated from the line-shape analysis is 5.2 meV. According to the similar analysis, the binding energy for the QW is found to be 3.2 meV, in which we used the 2D density of states to analyze the line-shape. The reduced dimension in the QWR's leads to the enhancement of the binding energy. The PL line width of the QWR's is larger than that of the QW. At this moment, it is difficult to discuss quantitative contribution of homogeneous and inhomogeneous components in the PL of the QWR's and QW. We have ignored any inhomogeneous broadening in our description of the radiative lifetime.

From the line-shape analysis, we found that either  $XX$  or  $X^*$  could be the origin of the NPL. Next, we analyze time-resolved PL spectra in order to identify which of  $XX$  and  $X^*$  is the origin of the NPL. Temporal evolutions of spectrally integrated  $X$  PL and NPL intensities are shown in Fig. 7. Solid and open circles plot the  $X$  PL and NPL components, respectively. These data were obtained from analyzing the time-resolved PL spectra measured at 2.5 K under the excitation intensity of  $0.72 \mu\text{J}/\text{cm}^2$ . The  $X$  PL shows a rapid decay near 50 ps. In contrast to this, the NPL intensity grows slowly. It is considered that this slow rise indicates the dynamical properties of the  $XX$  or  $X^*$  formation. Open circles



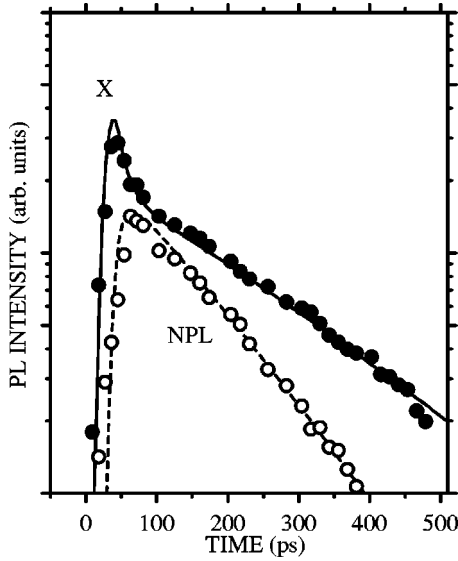


FIG. 7. Time-resolved X PL and NPL intensities of CdTe/Cd<sub>0.74</sub>Mg<sub>0.26</sub>Te QWR's, where solid and open circles are the plot of X PL and NPL components, respectively. Solid and dashed curves show calculated temporal evolution of the X PL and XX PL intensities.

in Fig. 8 shows the ratio between the X PL and NPL intensities shown in Fig. 7. The experimental data show a super linear dependence. We compare the experimental data with calculated results from rate equations of XX and X\*. In the case of XX formation and its dissociation processes, the rate equations for dynamics are given by<sup>39-41</sup>

$$\frac{dn_X}{dt} = J - \frac{n_X}{\tau_X} + \frac{n_{XX}}{\tau_{XX}} - 2k_+n_X^2 + 2k_-n_{XX}, \quad (4)$$

$$\frac{dn_{XX}}{dt} = -\frac{n_{XX}}{\tau_{XX}} + k_+n_X^2 - k_-n_{XX}, \quad (5)$$

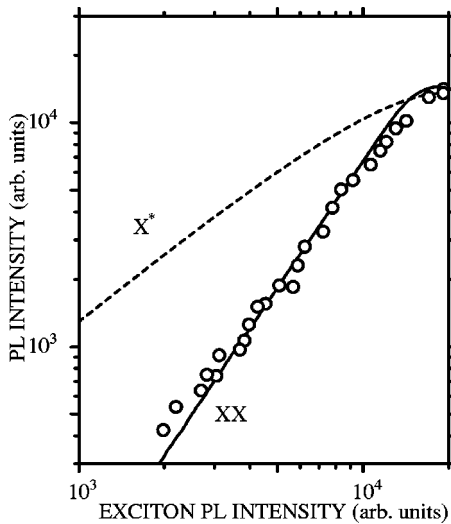


FIG. 8. NPL intensity versus the X PL intensity obtained from the decay profiles shown in Fig. 7, where solid and dashed curves show the calculated results for XX and X\* models, respectively.

where  $J$  is the generation rate of the  $X$ ,  $n_X$  ( $n_{XX}$ ) the density of the  $X$  ( $XX$ ),  $\tau_X$  ( $\tau_{XX}$ ) radiative lifetime of the  $X$  ( $XX$ ), and  $k_+$  and  $k_-$  the formation and dissociation velocities of the  $XX$ , respectively. Here we assume that the interconversion time between  $X$  and  $XX$  is much shorter than their radiative decay. On the other hand,  $X^*$  formation and its dissociation processes can be described by an atomic or chemical equation  $X + e^* \leftrightarrow X^*$ , where  $e^*$  is an electron or hole.<sup>50</sup> The  $X^*$  recombination leaves an electron or hole as an intermediate state. Therefore, the rate equations for the  $X^*$  model are expressed as

$$\frac{dn_X}{dt} = J - \frac{n_X}{\tau_X} - K_+n_{e^*}n_X + K_-n_{X^*}, \quad (6)$$

$$\frac{dn_{X^*}}{dt} = -\frac{n_{X^*}}{\tau_{X^*}} + K_+n_{e^*}n_X - K_-n_{X^*}, \quad (7)$$

where  $n_{X^*}$  and  $\tau_{X^*}$  are the density and radiative lifetime of the  $X^*$ , respectively,  $n_{e^*}$  the density of the electron or hole, and  $K_+$  and  $K_-$  the formation and dissociation velocities of the  $X^*$ , respectively. Furthermore, the dynamics of  $n_{e^*}$  is expressed as

$$\frac{dn_{e^*}}{dt} = J_{e^*} + \frac{n_{X^*}}{\tau_{X^*}} - K_+n_{e^*}n_X + K_-n_{X^*}, \quad (8)$$

where  $J_{e^*}$  is the photogeneration rate of the electron or hole. To interpret the observed data in Fig. 8, we tried to fit the data with the  $XX$  model [Eqs. (4) and (5)] and the  $X^*$  model [Eqs. (6)–(8)]. The observed superlinear dependence agrees well with the  $XX$  model. A solid line in Fig. 8 is the best fit result. The  $k_+$  and  $k_-$  parameters used here are  $1.0 \times 10^{-2}$  cm/s and  $4 \times 10^{11}$  s<sup>-1</sup>, respectively. However, since the generation rate of the  $X$  cannot be determined quantitatively, the  $k_+$  and  $k_-$  cannot be stated exactly. On the other hand, in the case of the  $X^*$  model, even if some parameters vary, the  $X^*$  PL intensity does not show the super linear dependence. A dashed line in Fig. 8 is a typical result obtained from Eqs. (6)–(8) for the  $X^*$  model.

Solid and dashed curves in Fig. 7 show the temporal evolution of the X PL and XX PL intensities calculated from Eqs. (4) and (5) in which we used the parameters obtained from the fitting in Fig. 8. Equations (4) and (5) hold for pulsed excitation only where the interconversion time between  $X$  and  $XX$  is much shorter than their radiative decay. The good agreement of the calculated results with the measured data indicates that the interconversion time between  $X$  and  $XX$  is indeed short. The estimated  $X$  and  $XX$  radiative lifetimes are 150 and 75 ps, respectively. It is generally known from the analysis of kinetics in the case of quasiequilibrium between the  $X$  and  $XX$  that the radiative lifetime of the  $XX$  is one-half of that of the  $X$ .<sup>39,41</sup> The observed result is consistent with the  $XX$  model. The obtained  $X$  radiative lifetime at 2.5 K together with analyzed lifetimes at 1.8 and 3.6 K are plotted in Fig. 3 by open circles. Whereas the total decay profile including the  $X$  and  $XX$  components deviates from the  $T^{1/2}$  dependence at  $\approx 10$  K, the extracted radiative

lifetime of the  $X$  obeys the  $T^{1/2}$  dependence even at  $\leq 10$  K, confirming the 1D nature in  $X$  thermalization.

#### IV. CONCLUSION

Excitonic luminescence from CdTe/Cd<sub>0.74</sub>Mg<sub>0.26</sub>Te QWR's grown on vicinal substrate was investigated. It was found that the observed radiative lifetimes in the QWR's and the QW are expressed as  $100 T^{1/2}$  ps K<sup>-1/2</sup> and  $11 T$  ps K<sup>-1</sup>, respectively. The estimated  $\tau_0$  found to be 72 ps (1D) and 5 ps (2D). The large  $\tau_0$  in the QWR's is due to the decrease of the  $X$ -coherence length imposed by the lateral confinement in the QWR's. With increasing the tilt angle  $\theta$  of the QWR's, the  $X$ -coherence length becomes long, and then the  $\tau_0$  reduces. At low temperature  $\leq 10$  K, however, the radiative lifetimes in the QWR's deviate from the  $T^{1/2}$  dependence. In this temperature range, a NPL appears at the lower energy side of the  $X$  PL. This NPL is enhanced at high excitation intensity. We focused on the  $XX$  and  $X^*$  forma-

tions and analyzed the NPL. From the line-shape analysis,  $XX$  or  $X^*$  is a possible origin of the NPL. The estimated binding energy is 5.2 meV. To confirm the origin of the NPL, we analyzed time-resolved PL spectra. The experimental data were compared with the calculation using the rate equations for the  $XX$  and  $X^*$  models. According to this analysis, it was concluded unambiguously that the observed NPL is due to the  $XX$  recombination. Furthermore, the evaluated radiative lifetimes for  $X$  obey the  $T^{1/2}$  dependence also at  $\leq 10$  K.

#### ACKNOWLEDGMENTS

We would like to acknowledge M. Nakayama, Osaka City University for fruitful discussions. This work was supported by the Photonics Materials Laboratory Project of the Graduate School of Science and Technology at Kobe University and in part by the Scientific Research Grant-in-Aid from the Ministry of Education, Science, and Culture, Japan.

\*Electronic address: 988d873n@kobe-u.ac.jp

<sup>1</sup>Y. Arakawa and H. Sakaki, Appl. Phys. Lett. **40**, 939 (1982).

<sup>2</sup>H. Temkin, G. J. Dolan, M. B. Panish, and S. N. G. Chu, Appl. Phys. Lett. **50**, 413 (1987).

<sup>3</sup>Y. Z. Hu, M. Lindberg, and S. W. Koch, Phys. Rev. B **42**, 1713 (1990).

<sup>4</sup>P. Ils, M. Michel, A. Forchel, I. Gyuro, M. Klenk, and E. Zielinski, Appl. Phys. Lett. **64**, 496 (1994).

<sup>5</sup>J. Christen, E. Kapon, E. Colas, D. M. Hwang, L. M. Schiavone, M. Grundmann, and D. Bimberg, Surf. Sci. **267**, 257 (1992).

<sup>6</sup>J. Christen, M. Grundmann, E. Kapon, E. Colas, D. M. Hwang, and D. Bimberg, Appl. Phys. Lett. **61**, 67 (1992).

<sup>7</sup>H. Akiyama, S. Koshiba, T. Someya, K. Wada, H. Noge, Y. Nakamura, T. Inoshita, A. Shimizu, and H. Sakaki, Phys. Rev. Lett. **72**, 924 (1994).

<sup>8</sup>D. Y. Oberli, M. A. Dupertuis, F. Reinhardt, and E. Kapon, Phys. Rev. B **59**, 2910 (1999).

<sup>9</sup>D. Gershoni, M. Katz, W. Wegscheider, L. N. Pfeiffer, R. A. Logan, and K. West, Phys. Rev. B **54**, 1872 (1996).

<sup>10</sup>D. Brinkmann, G. Fishman, C. Gourgon, Le Si Dang, A. Loffler, and H. Mariette, Phys. Rev. B **50**, 8930 (1994).

<sup>11</sup>W. Langbein, H. Gislason, and J. M. Hvam, Phys. Rev. B **60**, 16 667 (1999).

<sup>12</sup>P. Dua, S. L. Cooper, A. C. Chen, and K. Y. Cheng, Appl. Phys. Lett. **69**, 2261 (1996).

<sup>13</sup>R. Notzel, N. N. Ledentsov, L. Daweritz, K. Ploog, and M. Hohenstein, Phys. Rev. B **45**, 3507 (1992).

<sup>14</sup>R. Notzel, N. N. Ledentsov, and K. Ploog, Phys. Rev. B **47**, 1299 (1993).

<sup>15</sup>P. M. Petroff, A. C. Gossard, R. A. Logan, and W. Wiegmann, Appl. Phys. Lett. **41**, 635 (1982).

<sup>16</sup>P. M. Petroff, A. C. Gossard, and W. Wiegmann, Appl. Phys. Lett. **45**, 620 (1984).

<sup>17</sup>H. Kanbe, A. Chavez-Pirson, H. Ando, H. Saito, and T. Fukui, Appl. Phys. Lett. **58**, 2969 (1991).

<sup>18</sup>J. H. Hartmann, M. Charleux, J. Cibert, and H. Mariette, Appl. Phys. Lett. **72**, 3151 (1998).

<sup>19</sup>For example, M. Sugawara, in *Semiconductors and Semimetals*, edited by R. K. Willardson and Eicke R. Weber (Academic Press, New York, 1999).

<sup>20</sup>J. Feldmann, G. Petter, E. O. Gobel, P. Dawson, K. Moore, C. Foxon, and R. J. Elliott, Phys. Rev. Lett. **59**, 2337 (1987).

<sup>21</sup>L. C. Andreani, F. Tassone, and F. Bassani, Solid State Commun. **77**, 641 (1991).

<sup>22</sup>A. Polhmann, R. Hellmann, E. O. Gobel, D. R. Yakovlev, W. Ossau, A. Waag, R. N. Bicknell-Tassius, and G. Landwehr, Appl. Phys. Lett. **61**, 2929 (1992).

<sup>23</sup>J. Martinez-Pastor, A. Vinattieri, L. Carraresi, M. Colocci, Ph. Roussignol, and G. Weimann, Phys. Rev. B **47**, 10 456 (1993).

<sup>24</sup>I. Lawrence, W. W. Ruhle, G. Feuillet, H. Tuffigo, H. Mariette, C. Bodin, and J. Cibert, J. Phys. (France) **IV-C5**, 405 (1993).

<sup>25</sup>D. S. Citrin, Phys. Rev. Lett. **69**, 3393 (1992).

<sup>26</sup>B. Kuhn-Heinrich, W. Ossau, H. Heinke, F. Fischer, T. Litz, A. Waag, and G. Landwehr, Appl. Phys. Lett. **63**, 2932 (1992).

<sup>27</sup>L. Marsal, A. Wasiela, G. Fishman, H. Mariette, F. Michelini, S. Nagahara, and T. Kita, Phys. Rev. B **63**, 165 304 (2001).

<sup>28</sup>J. M. Hartmann, M. Charleux, J. Cibert, and H. Mariette, Appl. Phys. Lett. **72**, 3151 (1998).

<sup>29</sup>H. Ando, S. Nojima, and H. Kanbe, J. Appl. Phys. **74**, 6383 (1993).

<sup>30</sup>T. Sogawa, S. Ando, H. Ando, and H. Kanbe, Appl. Phys. Lett. **68**, 364 (1996).

<sup>31</sup>S. Nagahara, T. Kita, O. Wada, L. Marsal, and H. Mariette (unpublished).

<sup>32</sup>C. F. Klingshirn, *Semiconductor Optics* (Springer, Berlin, 1997), p. 361.

<sup>33</sup>R. Cingolani, Y. Chen, and K. Ploog, Phys. Rev. B **38**, 13 478 (1988).

<sup>34</sup>R. T. Phillips, D. J. Lovering, G. J. Denton, and G. W. Smith, Phys. Rev. B **45**, 4308 (1992).

<sup>35</sup>D. Birkedal, J. Singh, V. G. Lyssenko, J. Erland, and J. M. Hvam, Phys. Rev. Lett. **76**, 672 (1995).

<sup>36</sup>M. Nakayama, K. Suyama, and H. Nishimura, Phys. Rev. B **51**, 7870 (1995).

- <sup>37</sup>H. Ichida and M. Nakayama, Phys. Rev. B **63**, 195 316 (2001).
- <sup>38</sup>L. Besombes, K. Kheng, and D. Martrou, Phys. Rev. Lett. **85**, 425 (2000).
- <sup>39</sup>P. L. Gourley and J. P. Wolfe, Phys. Rev. B **20**, 3319 (1979).
- <sup>40</sup>P. L. Gourley and J. P. Wolfe Phys. Rev. B **25**, 6338 (1982).
- <sup>41</sup>J. C. Kim, D. R. Wake, and J. P. Wolfe, Phys. Rev. B **50**, 15 099 (1994).
- <sup>42</sup>P. Chen, J. E. Nicholls, M. O'Neill, T. Stirner, J. H. C. Hogg, B. Lunn, and D. E. Ashenford, J. Appl. Phys. **84**, 5621 (1998).
- <sup>43</sup>Y. Yamada, T. Yamamoto, S. Nakamura, T. Taguchi, F. Sasaki, S. Kobayashi, and T. Tani, Appl. Phys. Lett. **69**, 88 (1996)
- <sup>44</sup>A. Manassen, E. Cohen, A. Ron, E. Linder, and L. N. Pfeiffer, Phys. Rev. B **54**, 10 609 (1996).
- <sup>45</sup>A. Esser, E. Runge, R. Zimmermann, and W. Langbein, Phys. Rev. B **62**, 8232 (2000).
- <sup>46</sup>D. Sanvitto, R. A. Hogg, A. J. Shields, D. M. Whittaker, M. Y. Simmons D. A. Ritchie, and M. Pepper, Phys. Rev. B **62**, R13 294 (2000).
- <sup>47</sup>V. Ciulin, P. Kossacki, S. Haacke, J. D. Ganiere, B. Deveaud, A. Esser, M. Kutrowski, and T. Wojtowicz, Phys. Rev. B **62**, R16 310 (2000).
- <sup>48</sup>C. Y. Hu, W. Ossau, P. H. Tan, T. Wojtowicz, G. Karczewski, and J. Kossut, Phys. Rev. B **63**, 45 313 (2001).
- <sup>49</sup>E. Hanamura, J. Phys. Soc. Jpn. **39**, 1516 (1975).
- <sup>50</sup>J. Siviniant, D. Scalbert, A. V. Kavokin, D. Coquillat, and J.-P. Lascaray, Phys. Rev. B **59**, 1602 (1999).